



**HAL**  
open science

# Reducing the Uncertainty in the Satellite Altimetry Estimates of Global Mean Sea Level Trends Using Highly Stable Water Vapor Climate Data Records

Anne Barnoud, Bruno Picard, Benoît Meyssignac, Florence Marti, Michaël Ablain, Rémy Roca

► **To cite this version:**

Anne Barnoud, Bruno Picard, Benoît Meyssignac, Florence Marti, Michaël Ablain, et al.. Reducing the Uncertainty in the Satellite Altimetry Estimates of Global Mean Sea Level Trends Using Highly Stable Water Vapor Climate Data Records. *Journal of Geophysical Research. Oceans*, 2023, 128 (3), pp.e2022JC019378. 10.1029/2022jc019378 . hal-04235693

**HAL Id: hal-04235693**

**<https://hal.science/hal-04235693>**

Submitted on 10 Oct 2023

**HAL** is a multi-disciplinary open access archive for the deposit and dissemination of scientific research documents, whether they are published or not. The documents may come from teaching and research institutions in France or abroad, or from public or private research centers.

L'archive ouverte pluridisciplinaire **HAL**, est destinée au dépôt et à la diffusion de documents scientifiques de niveau recherche, publiés ou non, émanant des établissements d'enseignement et de recherche français ou étrangers, des laboratoires publics ou privés.

**Key Points:**

- The wet troposphere correction is responsible for 10% of the uncertainty of the global mean sea level (GMSL) over the altimetry era and for 40% over the last decade
- Using water vapor climate data records increases the GMSL estimate by 6% and reduces its uncertainty by 9%
- The Jason-3 radiometer is likely drifting by  $\sim -0.5 \text{ mm.yr}^{-1}$ , meaning the current estimate of GMSL rise is overestimated

**Correspondence to:**

A. Barnoud,  
[anne.barnoud@magellium.fr](mailto:anne.barnoud@magellium.fr)



**Citation:**

Barnoud, A., Picard, B., Meyssignac, B., Marti, F., Ablain, M., & Roca, R. (2023). Reducing the uncertainty in the satellite altimetry estimates of global mean sea level trends using highly stable water vapor climate data records. *Journal of Geophysical Research: Oceans*, 128, e2022JC019378. <https://doi.org/10.1029/2022JC019378>

Received 10 OCT 2022

Accepted 20 FEB 2023

## Reducing the Uncertainty in the Satellite Altimetry Estimates of Global Mean Sea Level Trends Using Highly Stable Water Vapor Climate Data Records

Anne Barnoud<sup>1</sup> , Bruno Picard<sup>2</sup> , Benoît Meyssignac<sup>3</sup> , Florence Marti<sup>1</sup> , Michaël Ablain<sup>1</sup> , and Rémy Roca<sup>3</sup> 

<sup>1</sup>Magellium, Ramonville-Saint-Agne, France, <sup>2</sup>Fluctus, Rabastens, France, <sup>3</sup>LEGOS, Université de Toulouse, CNES, CNRS, UPS, IRD, Toulouse, France

**Abstract** The global mean sea level (GMSL) has risen by  $3.3 \pm 0.2 \text{ mm.yr}^{-1}$  (68% confidence level) over 1993–2021. The wet troposphere correction (WTC) used to compute the altimetry-based mean sea level data is known to be a large source of error in the GMSL long-term stability. The WTC is derived from the microwave radiometers (MWR) on board the altimetry missions. In order to improve the long-term estimates of the GMSL, we propose an alternative WTC computation based on highly stable climate data records (CDRs) of water vapor derived from independent MWR measurements on board meteorological satellites. A polynomial model is applied to convert water vapor to WTC. The CDR-derived WTC enables reducing the low frequency uncertainty of the WTC applied to the altimetry data, hence reducing the uncertainty of the GMSL trend estimate. Furthermore, over 2016–2021, the comparison of MWR-based with CDR-based WTC shows a likely drift of the Jason-3 MWR WTC on the order of  $-0.5 \text{ mm.yr}^{-1}$  that would lead to an overestimation of the GMSL trend from 2016.

**Plain Language Summary** The rise of sea level has been continuously and globally monitored since 1993 thanks to altimetry satellites. The altimetry signals are slowed down by the water vapor present in the atmosphere. This effect is corrected using the measurements of the radiometer instrument on board the altimetry satellites. However, a large uncertainty is associated with these measurements. In this study, we assess the impact of the water vapor correction on the estimate of the global mean sea level rise and we propose an alternative correction computed from high quality independent measurements provided by other satellite missions. Over the full altimetry period, this new correction slightly increases the mean estimate of the sea level rise with a reduced uncertainty. Besides, we identify a lack of long-term stability of the radiometer measurements from Jason-3 altimetry mission launched in 2016. The new water vapor correction allows to overcome this stability issue.

### 1. Introduction

The global mean sea level (GMSL) change is a key indicator for climate change. Since 1993, the GMSL has been continuously and globally monitored thanks to satellite altimetry. Over 1993–2021, it has risen by  $3.3 \pm 0.2 \text{ mm.yr}^{-1}$  (standard uncertainty corresponding to 68% confidence level) and a significant acceleration of  $0.12 \pm 0.04 \text{ mm.yr}^{-2}$  is observed (updated from Ablain et al., 2019). Present scientific questions related to climate change require more and more stringent uncertainty levels (e.g., Meyssignac, de Conto, et al., 2019). The current GMSL uncertainties are due to instrumental noise and instabilities, orbit determination, various geophysical corrections applied, switch of altimetry missions. Among these sources of errors, the wet troposphere correction (WTC) was identified as a major factor affecting the sea level rise estimated from altimetry data due to the lack of long-term stability (Ablain et al., 2019). The WTC accounts for the increase of the path delay in altimetric measurements due to the presence of water vapor in the troposphere. It is derived from brightness temperature measurements performed by the microwave radiometer (MWR) on board the altimetry satellites used as reference for the computation of the GMSL (TOPEX/Poseidon, Jason-1, Jason-2, and Jason-3). Unfortunately, each of the MWR for the reference altimetry missions suffered from instrumental drifts (Brown, 2013) that are not totally corrected by the vicarious calibration approach (more details in Section 3.1). The WTC uncertainty is taken into account in the GMSL error and uncertainty budget (Ablain et al., 2019). It is modeled by uncertainties with a standard deviation of  $0.2 \text{ mm.yr}^{-1}$  and correlated over periods of 5–10 years.

As an alternative to the altimeters' MWR WTC, the wet troposphere path delay can be computed from water vapor content through a polynomial fit (Keihm et al., 2000; Stum et al., 2011). This approach is of particular interest because high quality long-term stable water vapor data has recently become available. Indeed, climate data records (CDRs) of total column water vapor (TCWV), also known as total precipitable water, are derived from brightness temperature measured by the Special Sensor Microwave/Imager (SSM/I) and Special Sensor Microwave Imager/Sounder (SSMIS) missions of the United States Air Force Defense Meteorological Satellite Program. These data are stable high-quality long-term data suitable for climate studies. Schröder et al. (2016) estimate the CDR TCWV trend standard uncertainties as low as  $0.006 \text{ kg}\cdot\text{m}^{-2}\cdot\text{yr}^{-1}$  within  $60^{\circ}\text{S}$ – $60^{\circ}\text{N}$  and over 1988–2008 for the most stable data set. Using a first order conversion between TCWV and WTC (Thao et al., 2014), the uncertainty of the resulting WTC trend is expected to be four to five times lower than the current uncertainty considered for the onboard MWR (Ablain et al., 2019). The demonstrated stability of CDR TCWV data motivates the use of this data to compute an alternative WTC for altimetric data and to reassess the WTC long-term uncertainty affecting the altimetric data. Consequently, the long-term uncertainty of the GMSL trend is expected to be improved. The main objective of this study is therefore to rigorously verify and accurately quantify the reduction of uncertainties in the GMSL trend by using the WTC deduced from water vapor CDRs rather than the one derived from the MWRs on board altimetry satellites.

The paper is organized as follows. The data used to compute the WTC and GMSL records are listed in Section 2. The physical principle of the computation of WTC from water vapor is described in Section 3 with the underpinning assumptions. The methods used to compute CDR-derived global mean WTC (GMWTC), to compute the GMSL records and to propagate the uncertainties are described in Section 4. In Section 5, we present the results showing the impact of using the CDR-derived WTC on the GMSL in terms of trends and uncertainties. In Section 6, we assess the improvement brought by the CDR water vapor data on the GMWTC stability in the light of independent data.

## 2. Data

### 2.1. Data for the WTC Computation

#### 2.1.1. ERA5 Data for the Coefficients Estimation

To establish the relation between WTC and TCWV, we use the latest reanalysis ERA5 (Hersbach et al., 2019) provided by the European Center for Medium-Range Weather Forecasts (ECMWF) and available at the Copernicus Climate Change Service (C3S) operated by ECMWF on behalf of the European Union. Temperature and humidity profiles, used to compute the WTC, are given over 137 model pressure levels with a  $1^{\circ} \times 1^{\circ}$  spatial resolution. TCWV data are also given over a  $1^{\circ} \times 1^{\circ}$  grid. We use the data over a 10-year period, from January 2010 to December 2019. Only the data over the ocean surface are selected, using the land sea mask field included in the ERA5 data set. It is worth noting that ERA5 does rely on CDR, as it assimilates for instance the Climate Monitoring Satellite Application Facility Brightness Temperature Fundamental CDR (CM SAF BT FCDR, Fennig et al., 2017). Still, long-term WTC directly computed from ERA5 does not fulfill the GMSL strong requirements on temporal stability. As discussed by Gutenstein et al. (2021), even though a reanalysis is based on a unique assimilation scheme, the changes in the observing system have an impact at climate scales.

#### 2.1.2. CDRs TCWV

Two sources of CDRs providing monthly gridded data of TCWV over the ice-free oceans are used to compute the WTC using a polynomial model. First, the Remote Sensing Systems (2016) (REMSS) data Version 7.0 Release 1 are provided at  $1^{\circ} \times 1^{\circ}$  resolution until present through regular updates. Second, the Hamburg Ocean-Atmosphere Fluxes and Parameters from Satellite (HOAPS) data Version 4.0 (Andersson et al., 2017) are provided at  $0.5^{\circ} \times 0.5^{\circ}$  resolution until December 2014 by the European Organisation for the Exploitation of Meteorological Satellites (EUMETSAT) Satellite Application Facility on Climate Monitoring. The HOAPS and REMSS data sets are identified by Schröder et al. (2016) as the most stable CDR sources providing water vapor data.

Schröder et al. (2013) compared the monthly mean of HOAPS TCWV data with the EUMETSAT ERA-Interim and the Japan Meteorological Agency JRA re-analyses. The authors observe that the global mean absolute bias is below  $0.5 \text{ kg}\cdot\text{m}^{-2}$  and that the root mean square error is below  $2 \text{ kg}\cdot\text{m}^{-2}$  over 1991–2006. More recently, Schröder et al. (2016) has estimated the trends and uncertainties of REMSS and HOAPS TCWV based on

the method of Weatherhead et al. (1998). Trends are estimated to  $0.025 \pm 0.007 \text{ kg.m}^{-2}.\text{yr}^{-1}$  for HOAPS and  $0.034 \pm 0.006 \text{ kg.m}^{-2}.\text{yr}^{-1}$  for REMSS over 1988–2008 within  $60^\circ\text{N}$  and  $60^\circ\text{S}$  and using a  $2^\circ \times 2^\circ$  grid resolution.

## 2.2. Data for the GMSL Computation

### 2.2.1. Along-Track Altimetry Data

We use the delayed time Level-2+ along-track altimetric products version 3.0 released in 2021 and distributed by AVISO+ for the TOPEX/Poseidon, Jason-1, Jason-2, and Jason-3 reference missions. The products include sea level anomaly sampled at 1 Hz as well as the WTC derived from the MWR on board the altimetry satellites. These along-track products serve as the basis data for the AVISO+ GMSL data record (Ablain et al., 2019; Guérou et al., 2022) and for the computation of the Copernicus Climate Change Service (C3S) satellite sea level gridded product dedicated to climate change studies (Legeais et al., 2021).

### 2.2.2. Altimetry-Based GMSL Uncertainty Budget

We use the GMSL altimetry error and uncertainty budget established by Ablain et al. (2019). It includes inter-mission GMSL offset uncertainties, trend uncertainties (due to orbit determination, glacial isostatic adjustment correction, and TOPEX-A/B altimeter instabilities), high and medium frequency uncertainties correlated over periods of 1 year and shorter (due to altimeter noise, geophysical corrections, orbits, etc.) and low frequency uncertainties (due to WTC and gravity fields for orbits). The MWR-derived WTC stability was estimated around  $\pm 0.2 \text{ mm.yr}^{-1}$  by comparison between the different onboard altimeter satellite MWRs and with models (e.g., ECMWF) (Legeais et al., 2014; Thao et al., 2014). Ablain et al. (2019) modeled the corresponding uncertainty by a time correlated error with a correlation timescale  $\lambda$  of 5 years and a standard deviation  $\sigma$  of 1.1 mm applying a Gaussian attenuation model to calculate the autocovariance  $C$ :

$$C(t) = \sigma^2 \exp\left(-\frac{1}{2} \left(\frac{t}{\lambda}\right)^2\right) \quad (1)$$

where  $t$  is the time span.

The WTC uncertainty is modeled uniformly over the whole altimetric period by Ablain et al. (2019). However, it might be underestimated over the recent period from 2016 because the Jason-3 MWR-derived WTC has not been reprocessed yet by calibration against independent data (more details in Section 3.1).

## 3. From Water Vapor to Wet Troposphere Correction

This section describes the benefits of using the water vapor CDR (Section 3.1) and recalls the basic equations to compute the WTC from the atmosphere water vapor content (Section 3.2). The polynomial conversion model from Keihm et al. (2000) and Stum et al. (2011) is updated with recent data and the resulting WTC is verified against a reference WTC derived from a formulation taking into account the three-dimensional atmospheric variations (Section 3.3).

### 3.1. Benefits of the Use of CDRs TCWV

The atmosphere affects the propagation of the signal between the altimetry satellite and the sea surface. The presence of electron content in the ionosphere, dry gases molecules in the troposphere and water vapor in the troposphere delay the radar signal. The path delay is the integration along the signal path of the sum of the refractivities of each component of the atmosphere: ionosphere, dry gases, liquid water and water vapor. In this study, we focus on the wet troposphere path delay, due to water vapor, which is accounted for in the altimetry processing chain. By convention, the corrections are subtracted from the uncorrected sea surface height (orbit position minus range) measurements to obtain the sea level anomalies. Therefore, the WTC is a negative quantity.

The WTC is directly derived from measurements performed by an MWR on board the altimetry missions. The internal calibration of the MWR on board the reference missions TOPEX/Poseidon, Jason-1 and Jason-2 only relies on the stability of internal noise injection diodes. Yet those diodes suffered from strong drifts on each of those missions (Brown et al., 2006, 2007). The Jet Propulsion Laboratory (JPL) developed time-delayed external

calibration process (Autonomous Radiometer Calibration System) aiming at correcting for the drifts but with a limited impact on the long-term stability of the WTC, thus on the GMSL (Brown, 2013). It is based on vicarious calibrations for short-term corrections and comparison to reference sensors such as SSMI/S for end-of-life reprocessing. Jason-3 radiometer also suffers from diode drifts, but considering the limitation of the calibration scheme of the previous instruments, it benefits from a regular platform maneuver that provides cold sky measurements. During the first 1.5 years of the Jason-3 mission, the cold sky maneuvers were planned about every 2 months before being increased to every 30 days. However, being not yet fully reprocessed, it does not benefit from the SSMI/S adjustment and a residual drift may occur (Shannon Brown, personal communication).

The TCWV is obtained from Fundamental CDR (FCDR) of brightness temperature measured by SSMI/S missions. On the contrary to the MWR on board reference altimetry missions, the stability of the radiometers dedicated to the observation of the atmosphere as the SSMI/S series is insured by a two-point calibration at each scan (one hot calibration based on an internal load temperature and one cold calibration based on cold sky measurements): the long-term stability of the FCDR used to establish the CDR records benefits from this calibration scheme (Fennig et al., 2020).

In addition to the operational products, a climate-dedicated solution is proposed by Fernandes et al. (2021) to correct for the instrumental drifts: the GNSS-derived Path Delay Plus (GPD+) algorithm combines the observations from MWR, from ECMWF analysis and from SSMI/S to derive a stable WTC (Fernandes et al., 2021). The GPD+ solution is thus potentially compatible with the objective of this study in reducing the uncertainty on the GMSL. But in order to obtain a description of the uncertainties associated with a new WTC, it has been decided to propose an approach that is based on a direct conversion of the CDR TCWV products. Thanks to the Global Vapor (G-VAP) project within the Global Energy and Water Exchanges (GEWEX) initiative, the stability and the associated uncertainty of those products is well-documented and thoroughly compared to other reference data sets (Schröder et al., 2016). The direct conversion from TCWV to WTC allows a clear understanding of the propagation of this uncertainty through the whole processing chain.

### 3.2. Basic Relations

The path delay due to the lower atmosphere is the integration of the refractivity along the path of the electromagnetic waves. An accurate approach to compute the dry and wet troposphere corrections is based on a parameterization of atmospheric refractivity  $N$  (Kerr, 1951; Smith & Weintraub, 1953):

$$N = a_d \frac{p_d}{T} + a_w \frac{e}{T} + b_w \frac{e}{T^2} \quad (2)$$

where  $p_d$  is the partial pressure of dry air,  $e$  the partial pressure of water,  $T$  the temperature. The contribution of cloud liquid water to atmospheric refractivity is neglected with an impact of less than 5 mm on the WTC under cloudy conditions (Goldhirsh & Rowland, 1982). For years, the values of the parameters  $a_d$ ,  $a_w$ , and  $b_w$  have been updated and discussed in the literature (Bean & Dutton, 1966; Bevis et al., 1994; Schelleng et al., 1933; Smith & Weintraub, 1953). The parameterization of Rüeger (2002) is used in this paper, with less than 1 mm impact on the WTC compared to Bevis et al. (1994) (not shown here). Integrating the refractivity  $N$  (Equation 2) along the path and separating the dry and wet components of the refractivity, the parametric formulation of the WTC is the following (Davis et al., 1985):

$$WTC = 10^{-6} \frac{R_v}{g_m} \left[ \left( a_w - \frac{R_d}{R_v} a_d \right) \int_0^{p_{\text{SFC}}} p dp + b_w \int_0^{p_{\text{SFC}}} \frac{q}{T} dp \right] \quad (3)$$

where  $R_d$  and  $R_v$  are respectively the specific gas constant for dry and wet air,  $q$  is the specific humidity in  $\text{kg} \cdot \text{kg}^{-1}$ ,  $p_{\text{SFC}}$  is the pressure at the surface and

$$g_m = g_0 (1 - 0.00265 \cos 2\varphi - 0.28 \cdot 10^{-6} H) \quad (4)$$

is defined by Davis et al. (1985) as the acceleration due to mass at the center of mass of the vertical column with  $g_0 = 9.784 \text{ m} \cdot \text{s}^{-1}$ ,  $\varphi$  the geodetic latitude and  $H$  the altitude in meters. Equation 3 therefore allows us to accurately assess the WTC by taking into account the three-dimensional atmospheric variations. This computation requires a high computational cost and the use of large data sets. We use Equation 3 to estimate a 3D integrated

**Table 1**

Total Column Water Vapor to Wet Troposphere Correction Polynomial Coefficients Estimations and Their Standard Uncertainties, and Comparison With the Coefficients From the Literature (Keihm et al., 2000; Stum et al., 2011)

	$a_0$ [m.(kg.m <sup>-2</sup> ) <sup>-1</sup> ]	$a_1$ [m.(kg.m <sup>-2</sup> ) <sup>-2</sup> ]	$a_2$ [m.(kg.m <sup>-2</sup> ) <sup>-3</sup> ]	$a_3$ [m.(kg.m <sup>-2</sup> ) <sup>-4</sup> ]
Keihm et al. (2000)	6.759e-3	-2.91e-5	3.1e-6	
Stum et al. (2011)	6.8544e-3	-4.377e-4	7.14e-5	-3.8e-6
This study	7.1066e-3 ± 6.088e-5	-6.815e-5 ± 8.169e-6	1.597e-6 ± 2.792e-7	-1.204e-8 ± 2.715e-9

WTC as an accurate reference for validation. The objective here is to take advantage of the CDR TCWV data available to compute an alternative WTC for altimetric data. The computation of WTC directly from TCWV has already been proposed in the past. It has been used by Keihm et al. (2000) to validate the TOPEX/Poseidon radiometer WTC against SSM/I/S TCWV. Following the same approach, Stum et al. (2011) proposed to fit the ratio WTC/TCWV by a third degree polynomial leading to the following relation between WTC in meters and TCWV in kg.m<sup>-2</sup>:

$$WTC = (a_0 + a_1TCWV + a_2TCWV^2 + a_3TCWV^3)TCWV \quad (5)$$

Keihm et al. (2000) computed the polynomial coefficients from profiles measured by radiosondes while Stum et al. (2011) parameterization is estimated using the profiles from ECMWF analysis, with no further details on the processing or the time span. The  $a_{i,0 \leq i \leq 3}$  coefficient values obtained by Keihm et al. (2000) and Stum et al. (2011) are listed in Table 1. The estimation of the updated coefficients and of their standard uncertainties for the current study is detailed in the following paragraph.

### 3.3. Polynomial Fit and Associated Uncertainties

In order to establish the conversion between the CDR TCWV and a CDR-derived WTC, the quantities WTC and TCWV and the corresponding ratio are computed over the ocean for each grid cell of a 1° × 1° daily ERA5 analysis at 00:00 between 2010 and 2019. The TCWV is directly available from the ERA5 data set. The WTC is

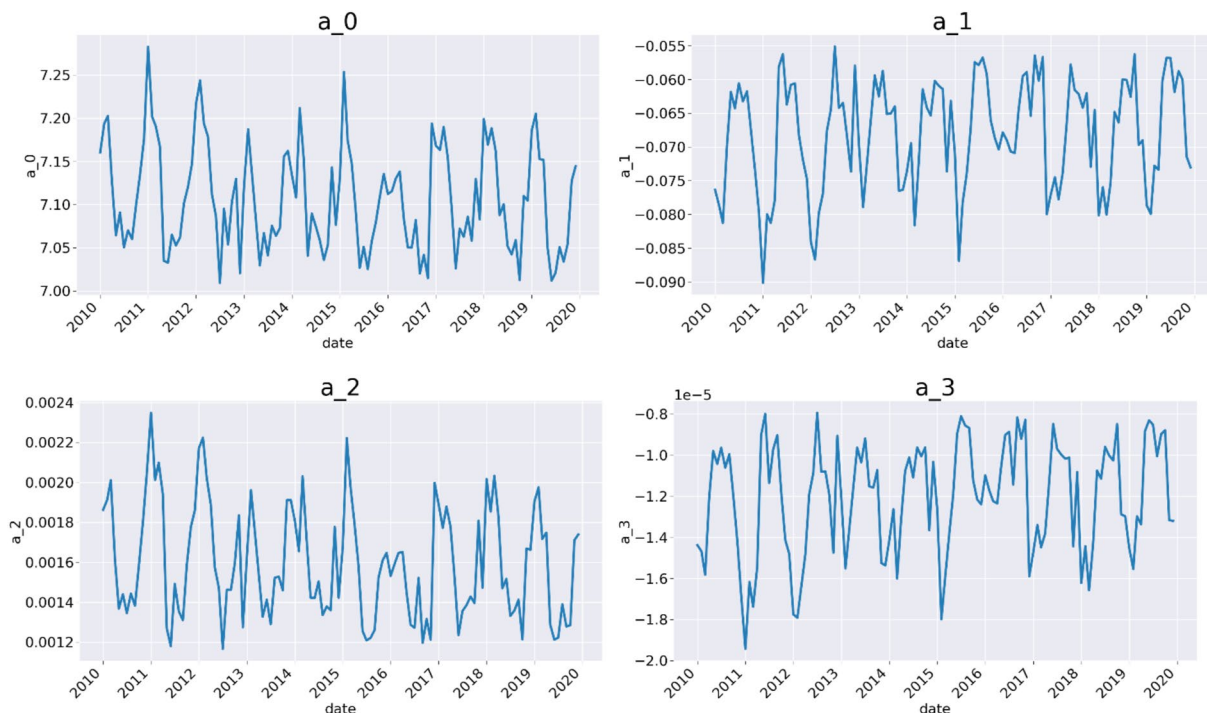


**Figure 1.** Temporal variation of the total column water vapor to wet troposphere correction monthly polynomial coefficients  $a_{i,0 \leq i \leq 3}$  over 2010–2019.

computed by integration as in Equation 3 and using the “best average” parametrization of Rieger (2002, Equation 10). One set of  $a_i$  parameters is fitted for each month over the global distribution of WTC/TCWV against TCWV, gathering a total of about 30 global grids.

Finally, in order to facilitate the processing of the already complex processing chain from WTC to GMSL, an additional simplification is applied to the computation of the WTC from the CDR TCWV. A single set of  $a_i$  coefficients is considered for the whole altimetry era, as the averaged value of each coefficient over the period 2010–2019. The CDR-derived WTC is eventually computed by applying this single set of averaged  $a_i$  coefficients for each grid cell of the monthly gridded CDR TCWV products. The step-by-step processing of the use of CDR TCWV and CDR-derived WTC in the computation of the GMSL is detailed in Section 4.1 “Computation of the GMWTC and GMSL from along-track data.”

In the following paragraphs, we will clarify and discuss the impact of the main assumptions in the conversion process onto the uncertainty of the WTC trend and propose a method to quantify this uncertainty. A more accurate approach would have consisted in computing independently a set of  $a_i$  coefficients for each grid cell and on a monthly basis over the whole altimetry era. Considering the complexity of such an approach in terms of data volume and since the current study is the first attempt to assess the impact of TCWV CDR on the reduction of the uncertainty on the GMSL, the simpler approach using a single set of averaged  $a_i$  coefficients has been selected. However, it may introduce artificial trends on the WTC computed from the CDRs. The evolution of the global warming over the last 30 years may have (a) an impact on the relation between WTC and TCWV since the relation with the temperature is only partially taken into account in Equation 5 when temporarily averaged values of  $a_i$  coefficients are considered over the whole period, as already pointed out by Keilm et al. (2000), and (b) a differential impact on specific regions with particular geophysical conditions (for instance upwelling areas) when geographically averaged values of  $a_i$  parameters are considered for the whole globe. This latter explains the variations of the seasonal and an interannual variation of the  $a_i$  coefficients illustrated by Figure 1. For instance, the  $a_0$  coefficient's variations show a  $0.2e-3 \text{ m} \cdot (\text{kg} \cdot \text{m}^{-2})^{-1}$  peak-to-peak amplitude which corresponds to a variation of about 3%.

In order to illustrate the direct impact on the trend, the WTC computed from the single averaged set of coefficients is compared to the reference being the more accurate solution established using Equation 3. Figure 2 shows the time series of the mean (left) and the standard deviation (right) of the difference between the two solutions. A three-monthly averaging is applied to time series in order to emphasize the temporal evolution. Note that some tests have been conducted (not shown here) using ERA5 analysis at a time different than 00:00, confirming that the potential diurnal signal on the WTC has a negligible impact on the computation of the GMWTC over the ocean, whether by integration or through the potential fit of TCWV.

The current study being focused on the uncertainty associated to the WTC trend, the impact of the WTC accuracy due to the polynomial solution is acceptable: the global standard deviation of the difference between the reference and the final polynomial approach is stable and smaller than 2.5 mm (see Figure 2, right).

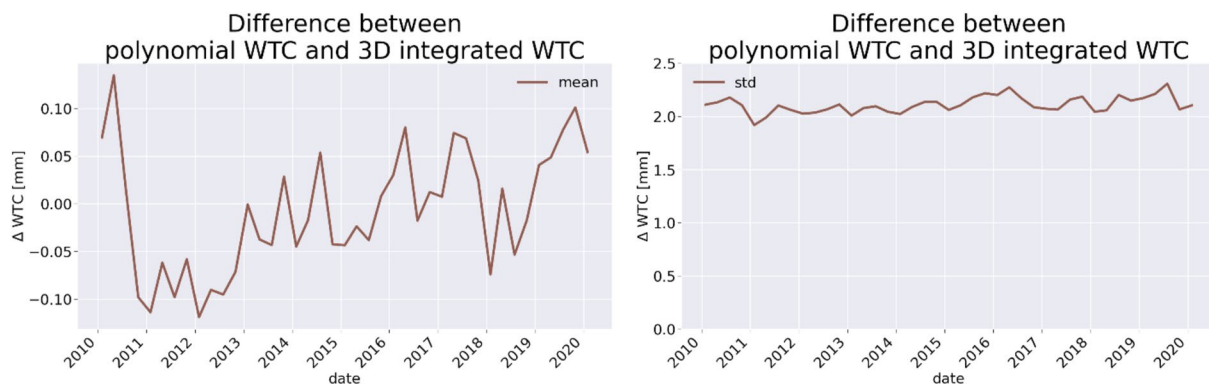


**Figure 2.** Time series of the differences of wet troposphere correction computed from the polynomial model updated in this study and the reference 3D integration. Left: mean. Right: standard deviation.

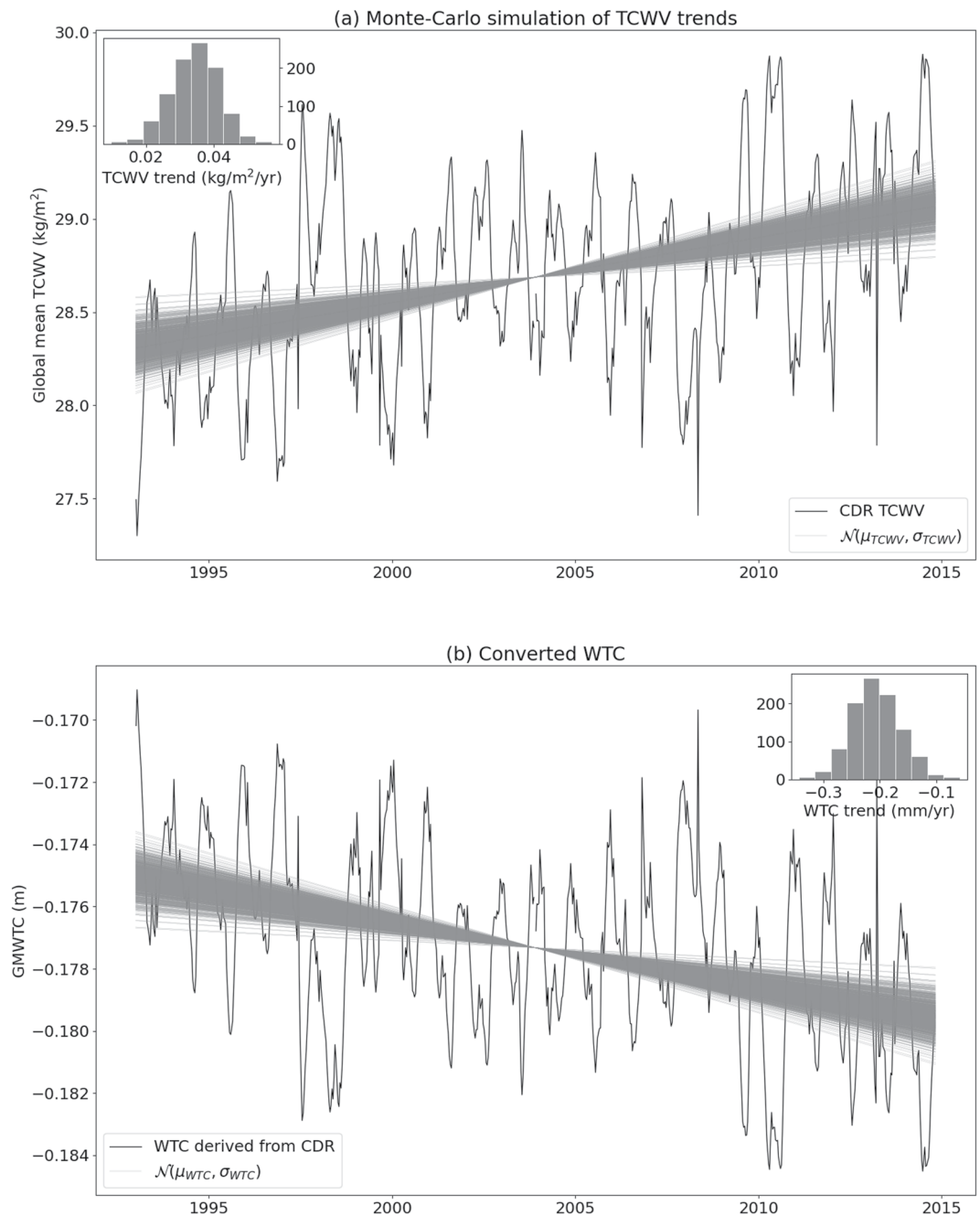


**Figure 3.** Monte-Carlo uncertainty propagation from REMSS CDR TCWV trend to global mean WTC trend. (a) Random simulations based on the TCWV trend uncertainty estimate from Schröder et al. (2016). Insert: distribution of TCWV trends. (b) Conversion to WTC. Insert: distribution of resulting WTC trends.

However the simplifications do introduce errors on the stability of the correction. Figure 2 (left) shows that the underlying assumption on the temporal stability of the relation between WTC and TCWV is not ensured over a 10 years period. Neglecting for the specific larger values in 2010, a positive trend of  $+0.02 \text{ mm}\cdot\text{yr}^{-1}$  is observed when using the average polynomial solution instead of the 3D integration between 2011 and 2019. It is not possible within the current study to determine whether this trend over less than 10 years represents an interannual trend compensated for over previous decades or partially the effect of the simplification assumptions. Further studies will be dedicated to this objective. Meanwhile, the potential error on the trend introduced by the simplifications is partially taken into account by the Monte-Carlo approach presented in the next section. The uncertainty on the



**Table 2**

Global mean WTC Trend Standard Uncertainties ( $\text{mm}\cdot\text{yr}^{-1}$ ) Due To the Total Column Water Vapor Data and  $a_i$  Polynomial Coefficients Uncertainties

Data set	Period	TCWV trend	TCWV bias	$a_0$	$a_1$	$a_2$	$a_3$	Total
REMSS	1993–2020	0.036	0.002	0.003	0.022	0.033	0.013	0.055
REMSS	1993–2014	0.035	0.001	0.002	0.019	0.027	0.010	0.049
HOAPS	1993–2014	0.043	0.001	0.002	0.017	0.025	0.009	0.053

Note. The total uncertainty is computed from the sum of variances, assuming all sources of uncertainty are independent.

final single set of  $a_i$  coefficients used to compute the CDR-derived WTC is defined as the variability (the standard deviation) of the monthly  $a_i$  over the 10 years period. It is worth noting that, if this approach introduces a large artificial trend on the CDR-derived WTC, it will necessarily be detected by the assessment exercise presented in Section 6, which consists of a consistency check of the GMWTCs computed from the CDR water vapor and from the MWR of various altimetry missions (see Figures 7 and 8).

## 4. Method to Implement the CDR-Derived WTC in the GMSL Computation

### 4.1. Computation of the GMWTC and GMSL From Along-Track Data

The workflow to compute the GMWTC and GMSL involves three main steps: (a) the interpolation of TCWV along the altimetry tracks, (b) the gridding of along-track data and the computation of the global means and (c) the combination of high and low GMWTC frequencies to avoid collocation errors. Each step is described below in more detail.

The monthly gridded TCWV data are interpolated at the locations and times of the Level-2+ along-track altimetry data (step 1). This is performed by trilinear spatio-temporal interpolation. The obtained along-track TCWV are then converted into along-track WTC using Equation 5. Consequently, both the MWR-based and CDR-derived WTCs are available to compute the sea level anomaly from the Level-2+ products.

To compute global means from along-track data (step 2), we follow the same procedure as documented by AVISO+ ([www.aviso.altimetry.fr](http://www.aviso.altimetry.fr)). For each altimetry mission, we compute  $3^\circ \times 1^\circ$  resolution grids per cycle of 10 days from along-track data of WTC and sea level anomaly, using both MWR and CDR data. In each cell, we average only the data where the MWR WTC is available and where there is the validation flag in the Level-2+ data so that the WTC and mean sea level grids are computed using the same data coverage. The global mean time series are computed using spatial averages weighted by the latitude and by the ratio of water-covered cell-surface within  $66^\circ\text{S}$  and  $66^\circ\text{N}$ . In addition, we correct for the inter-mission offsets between two consecutive missions (e.g., TOPEX/Jason-1, Jason-1/Jason-2, Jason-2/Jason-3), except for the CDR-derived GMWTC which is not affected by the altimetry mission switches. Each offset is computed over specific cycles selected within the tandem period, namely nine cycles starting from the seventh cycle of the substituting mission (Zawadzki & Ablain, 2016).

As the FCDR measurements are not colocalized in time and space with the along-track altimeter measurements and due to the monthly resolution of water vapor CDRs, the CDR-derived WTC interpolated at the position of the 1-Hz altimeter measurements does not contain high frequency content accurately enough. Therefore, we produce a GMWTC combining the high-frequencies from the MWR and the low-frequencies from the CDRs (step 3). To do so, a low-pass Lanczos filter with a 1-year cut-off frequency is applied to the MWR-based GMWTC and to the CDR-derived GMWTC. The 1-year cut-off frequency is chosen to be sufficiently high not to alter the high frequency content by the interpolated CDRs. This value could probably be reduced to a few months, but the sensitivity to the cut-off frequency has not been studied here as we focus on the impact of the WTC stability on longer time scales. The combined GMWTC (noted  $\text{GMWTC}_{\text{CDR\_LF+MWR\_HF}}$ ) is then obtained from the initial MWR-based GMWTC time series (noted  $\text{GMWTC}_{\text{MWR}}$ ), removing the MWR-based GMWTC low-frequencies ( $\text{GMWTC}_{\text{MWR\_LF}}$ ) and adding back the CDR-derived GMWTC low-frequencies ( $\text{GMWTC}_{\text{CDR\_LF}}$ ):

$$\text{GMWTC}_{\text{CDR\_LF+MWR\_HF}} = \text{GMWTC}_{\text{MWR}} - \text{GMWTC}_{\text{MWR\_LF}} + \text{GMWTC}_{\text{CDR\_LF}} \quad (6)$$

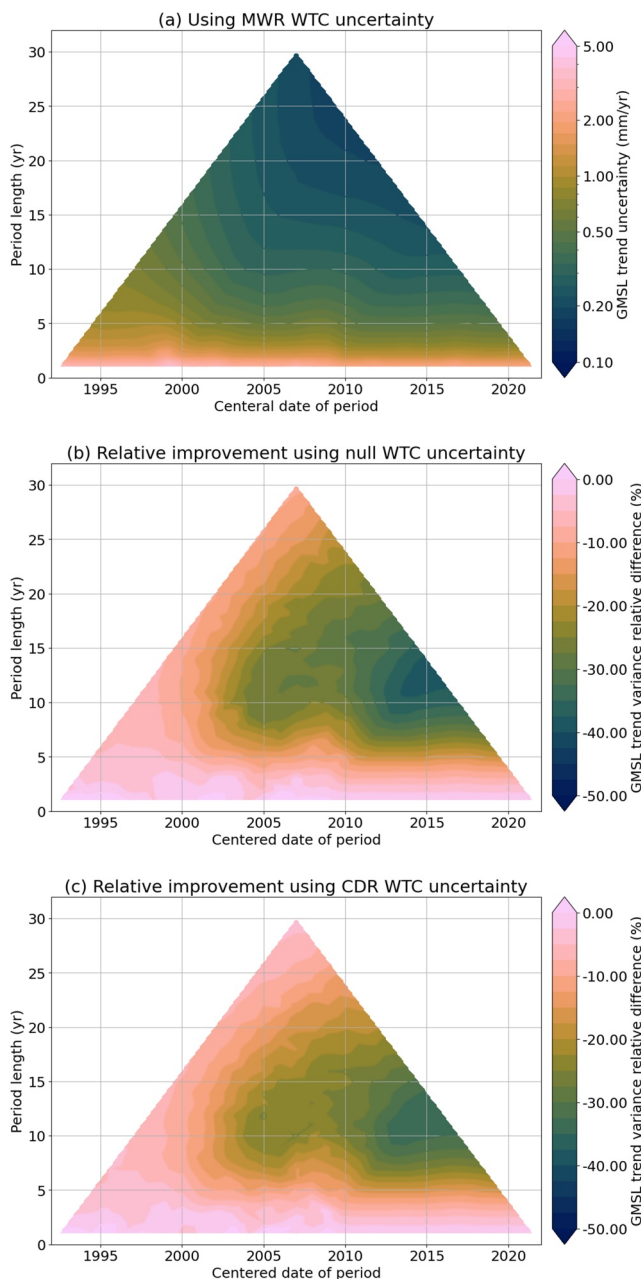


**Figure 4.** Uncertainty in global mean sea level (GMSL) trends. (a) Uncertainty in GMSL computed with a wet troposphere correction (WTC) derived from the altimeter microwave radiometers (MWR). (b) Relative variance difference using a null WTC uncertainty with respect to the MWR WTC uncertainty. This panel shows the maximum possible percentage of variance reduction when improving the WTC estimate. (c) Relative variance difference using the climate data record WTC uncertainty with respect to the MWR WTC uncertainty. In all panels the y-axis indicates the length of the period over which trends are computed. The x-axis indicates the date at the center of the period over which trends are computed.

The CDR-derived GMSL is then obtained by replacing the  $GMWTC_{MWR}$  by the  $GMWTC_{CDR\_LF+MWR\_HF}$ .

#### 4.2. Propagation of Uncertainties From TCWV to GMWTC and GMSL Trends

An estimation of the CDR-derived GMWTC trend uncertainty is required to assess the impact of the use of CDR water vapor data on long-term estimates of the GMSL. The uncertainties are propagated from TCWV to the GMWTC trend using an empirical approach. Monte-Carlo simulations are used to propagate the effects of the TCWV trend uncertainty (Figure 3), of the TCWV bias uncertainty and of the four  $a_i$  polynomial coefficients (Equation 5). The TCWV trend uncertainties are provided by Schröder et al. (2016) and the bias uncertainty is estimated by Schröder et al. (2013). The  $a_i$  polynomial coefficient uncertainties are estimated in this study (Table 1). Assuming that these sources of uncertainty are independent, we assess their effects independently using 1,000 simulations from a Gaussian distribution for each of these sources of uncertainty. The resulting GMWTC trends are normally distributed as well (see Figure 3 for the propagation of the TCWV trend as an example). The full GMWTC trend uncertainty is then obtained by summing the variances. By assuming that the sources of uncertainties are independent, we neglect potential correlations, in particular between the  $a_i$  coefficients, so that the resulting GMWTC trend uncertainty estimate may be considered as an upper bound of the actual GMWTC trend uncertainty.

The GMWTC and GMSL trend uncertainties are computed at any time over any period of time using the extended ordinary least squares method. We use the GMSL uncertainty budget from Ablain et al. (2019), replacing the WTC long-term uncertainty estimate as needed (e.g., MWR or CDR stability uncertainty).

### 5. Results

#### 5.1. Estimation of the CDR-Derived GMWTC Long Term Stability Uncertainty

Using the empirical approach detailed in Section 4.2, we estimate the CDR-derived GMWTC trend uncertainty over 1993–2020 (REMSS) and over 1993–2014 (REMSS and HOAPS). For the REMSS data set the TCWV trend uncertainty of  $0.006 \text{ kg.m}^{-2}.\text{yr}^{-1}$  (Schröder et al., 2016) results in a GMWTC trend uncertainty of about  $0.036 \text{ mm.yr}^{-1}$  (Table 2). For the HOAPS data set, the TCWV trend uncertainty of  $0.007 \text{ kg.m}^{-2}.\text{yr}^{-1}$  (Schröder et al., 2016) results in a GMWTC trend uncertainty of  $0.043 \text{ mm.yr}^{-1}$ . The GMWTC trend uncertainty due to the propagation of the TCWV bias is negligible. The GMWTC trend uncertainty due to the  $a_i$  polynomial coefficient uncertainties varies with the considered period and data set, but the relative importance of each coefficient is the same:  $a_2$  and  $a_1$  contribute the most, followed by  $a_3$ , and  $a_0$  contribution is negligible (Table 2). The resulting total uncertainty on the CDR-derived GMWTC is estimated by summing the variances (i.e., assuming that the sources of uncertainties are independent) leading to an uncertainty of about  $0.052 [0.049\text{--}0.055] \text{ mm.yr}^{-1}$  depending on the period and on the data set. In practice, the  $a_i$  coefficients are likely to be correlated

so these values are likely overestimated. In the following, the CDR-derived GMWTC trend uncertainty used for the propagation to the GMSL is an uncorrelated uncertainty of  $0.05 \text{ mm.yr}^{-1}$ , regardless of the CDR data set used and period considered. Compared to the altimeters' MWR-based GMWTC uncertainty which amounts to

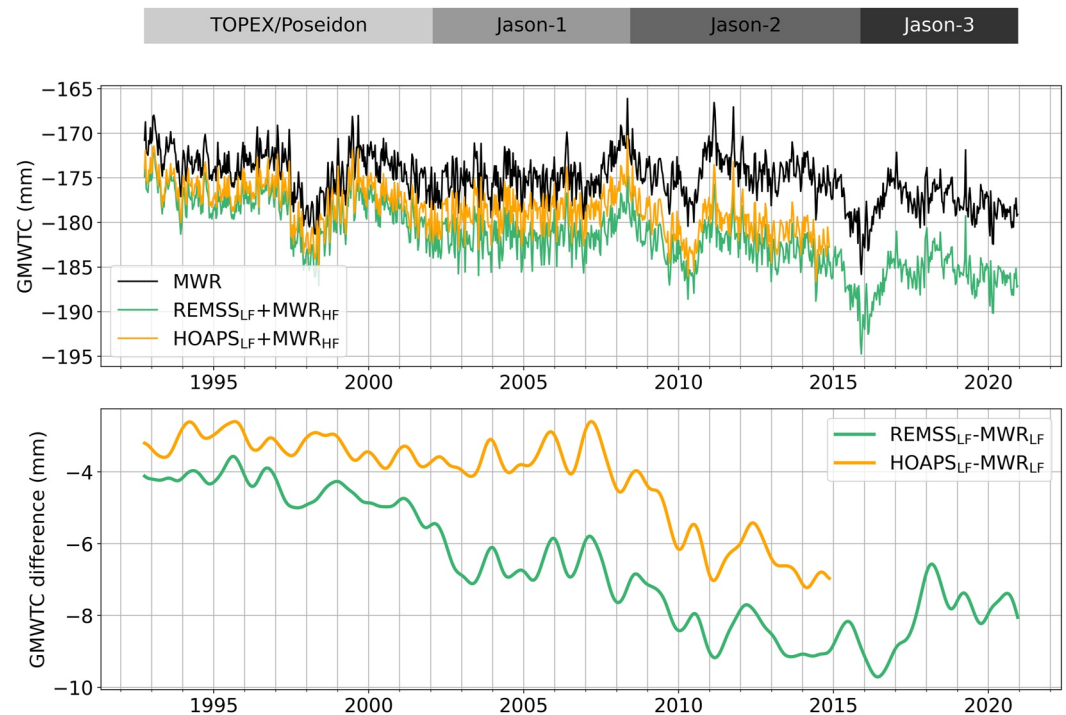


**Figure 5.** Comparison of altimeters' MWR-based, REMSS-derived and HOAPS-derived global mean WTC (GMWTC). Top: GMWTC time series. Bottom: differences between CDR-derived GMWTC and altimeters' MWR-based GMWTC. Negative trends in the GMWTC differences indicate that the global mean sea level (GMSL) corrected with the CDR-derived GMWTC increases faster than the GMSL corrected with the MWR-derived GMWTC. Positive trends in the GMWTC differences indicate that the GMSL corrected with the CDR-derived GMWTC increases more slowly than the GMSL corrected with the MWR-derived GMWTC.

$0.2 \text{ mm.yr}^{-1}$  for periods of 5 years (see Ablain et al., 2019), this is an uncertainty variance reduction of up to 94% (Table A1). For periods longer than 5 years, the correlation of the altimeters' MWR-based GMWTC errors results in lower uncertainties. Similarly, unestimated correlations in the CDR-derived GMWTC are also likely to lead to lower trend uncertainties over long periods of time.

## 5.2. Impact of the WTC Long-Term Stability Uncertainties on the Uncertainties in GMSL Trends

To assess the impact of the altimeters' MWR-based WTC long-term stability uncertainty on the GMSL data record, we compare the GMSL trend uncertainty for various WTC uncertainty estimates: with the MWR WTC uncertainty, with a null WTC uncertainty (ideal case) and with the CDR-derived WTC uncertainty estimated at  $0.05 \text{ mm.yr}^{-1}$  in the previous section. The reference GMSL trend uncertainty derived using the MWR WTC is shown on Figure 4a.

The relative variance reduction of the GMSL trend uncertainty when setting the WTC stability uncertainty to zero is shown on Figure 4b, quantifying the maximal percentage of variance reduction that could be reached if the WTC was perfectly stable. The percentage of variance reduction is low at high frequencies and increases with periods and time. The highest reductions are obtained during the Jason-2 and Jason-3 periods with a maximal reduction that approaches 40% for periods of about 10 years at the end of the altimetric period. During the TOPEX/Poseidon period (1993–2002), the reduction mostly stands below 10% due to the larger contribution of other sources of uncertainty (mainly related to high frequency errors with correlations below 1 year and TOPEX side-A altimeter instabilities between 1993 and 1999, see Ablain et al., 2019). Over the whole altimetric period, the maximum possible percentage of variance reduction in trend uncertainty is around 10% (upper corner of Figure 4b).

Figure 4c shows the uncertainty variance reduction in GMSL trends when using a GMWTC trend uncertainty of  $0.05 \text{ mm.yr}^{-1}$  in the GMSL uncertainty budget instead of the MWR-based GMWTC uncertainty. As the

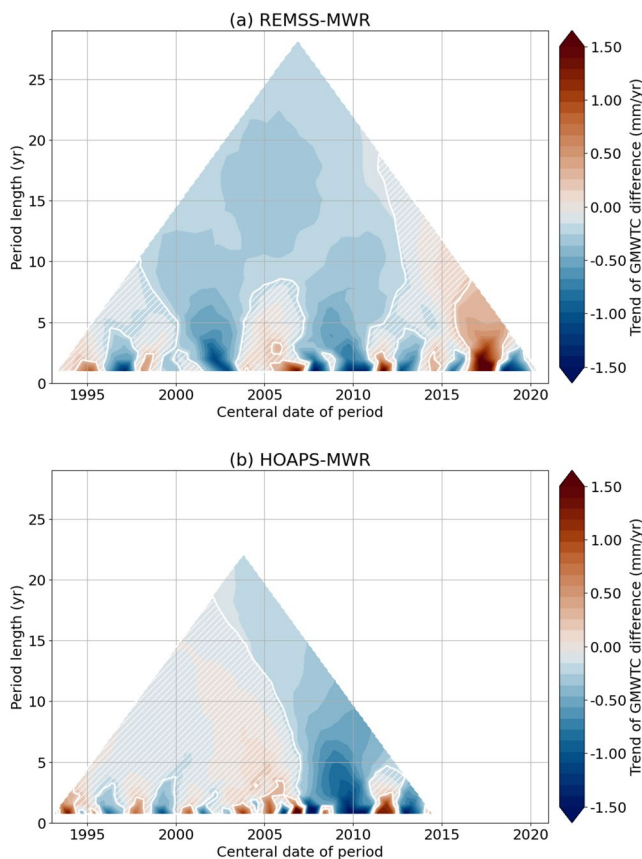


**Figure 6.** Trend of global mean WTC (GMWTC) differences between CDR-derived and MWR-based wet troposphere correction. Hatched areas correspond to non-significant trend differences with respect to the 68% confidence level (i.e., ratio of trend over trend standard uncertainty lower than 1). (a) Trend of  $GMWTC_{REMSS_{LF+MWR_{HF}}}-GMWTC_{MWR}$ . (b) Trend of  $GMWTC_{HOAPS_{LF+MWR_{HF}}}-GMWTC_{MWR}$ .

uncertainty variance reduction on the GMWTC trend uncertainty reaches 94% of the maximal possible reduction, Figure 4c is very similar Figure 4b where no GMWTC uncertainty was taken into account. The maximal uncertainty variance reduction is observed during the Jason-2 period with a reduction of up to 27% (Table A1). Over the full altimetry period (29 09 1992–28 06 2021), the trend of the GMSL variance is reduced by about 9% (Table A1).

### 5.3. Impact of the CDR-Derived GMWTC on the GMSL Trends

The GMWTCs computed from the altimetry mission MWR and derived from the CDRs (noted  $GMWTC_{REMSS_{LF+MWR_{HF}}}$  and  $GMWTC_{HOAPS_{LF+MWR_{HF}}}$  for REMSS and HOAPS data sets respectively) and their differences are shown on Figure 5. The trends of the GMWTC differences are computed over any period of time (1 year and longer) at any time over the time series (Figure 6). Figure 6 outlines the trends of the GMWTC differences that are significant with respect to their standard uncertainties. The quantified GMWTC trends and associated uncertainties are given in Table A1 for each individual altimetry mission and over the full altimetric period. Over 29 09 1992–07 11 2014, the CDR-derived GMWTC trends are consistent within standard uncertainty while they significantly differ from the  $GMWTC_{MWR}$  trend (Table A1). While the CDR-derived GMWTCs usually decrease faster than the  $GMWTC_{MWR}$ , the behavior of the GMWTC differences varies throughout the altimetry era (Figures 5 and 6). At the beginning of the altimetry period, the GMWTC differences do not show any significant trend. The difference between  $GMWTC_{HOAPS_{LF+MWR_{HF}}}$  and  $GMWTC_{MWR}$  shows a significant negative trend from the beginning of the Jason-2 period while the difference between  $GMWTC_{REMSS_{LF+MWR_{HF}}}$  and  $GMWTC_{MWR}$  shows a significant negative trend over both the Jason-1 and Jason-2 periods. Over Jason-3, the behavior changes with a significant positive trend in the difference between  $GMWTC_{REMSS_{LF+MWR_{HF}}}$  and  $GMWTC_{MWR}$ . We recall that no HOAPS data are available over the Jason-3 period for comparison as they are only available until the end of 2014. Consequently, using the CDR-derived WTC instead of the MWR-based WTC increases the GMSL trend by a few percents and up to about 10% depending on the CDR data set and period of time, except over Jason-3's period where it is reduced by about 8% (Table A1).

### 5.4. Assessment by Comparison With Independent MWR-Derived WTC Data Over the Jason-3 Period

Interestingly we find that the trend differences between the CDR-derived GMWTC (based on REMSS) and the MWR-derived GMWTC are stronger and positive over the recent years corresponding to the Jason-3 period (2016–2020, see Figure 6a and Table A1). To validate our results, we compare the results obtained over the Jason-3 period to the GMWTC derived from SARAL/AltiKa and Sentinel-3A altimetry missions that fly simultaneously with Jason-3 on different orbits. The positive trend difference of  $0.33 \pm 0.21 \text{ mm.yr}^{-1}$  in Table A1 is of the same sign as the WTC difference at crossovers between Sentinel-3A and Jason-3 MWRs ( $0.5 \text{ mm.yr}^{-1}$ ) and between SARAL/AltiKa and Jason-3 MWRs ( $0.8 \text{ mm.yr}^{-1}$ ) estimated by Barnoud et al. (2021). Following the approach of Jugier et al. (2022) adapted for the comparison of GMWTC trends, we estimate the GMWTC trend differences and associated uncertainties between CDR, Jason-3, SARAL/AltiKa and Sentinel-3A (Figure 7). Jason-3's MWR shows significant relative trend differences in all the comparisons. The CDRs appear to be more consistent with Sentinel-3A and SARAL/AltiKa than with Jason-3 data. These comparisons give confidence in the CDR-derived WTC and outline a likely drift of Jason-3's MWR. This conclusion is reinforced by the compar-

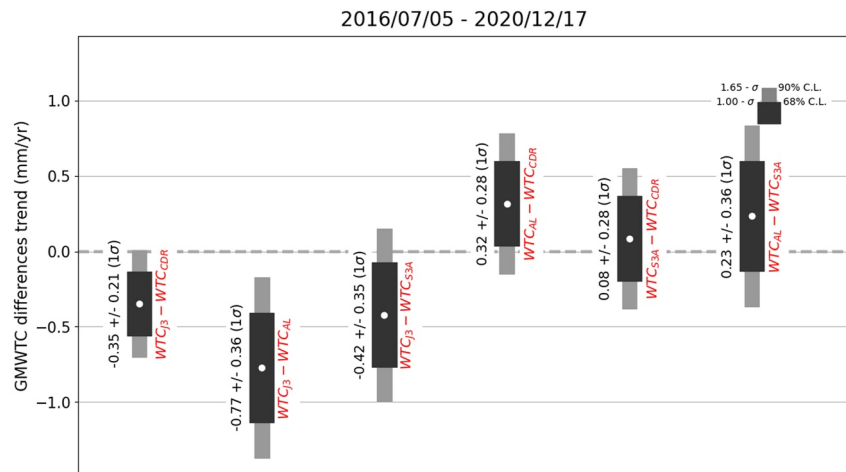


**Figure 7.** Comparison of global mean WTC (GMWTC) differences trends between Jason-3's MWR, REMSS CDR, SARAL/AltiKa's MWR (AL) and Sentinel-3A's MWR (S3A) over the period from 05 07 2016 to 17 12 2020. GMWTC differences trends impact the global mean sea level differences trends with the opposite sign. Intervals of 68% and 90% confidence levels are drawn, corresponding to 1 and 1.65 standard uncertainties ( $\sigma$ ).

ison of the GMWTC differences time series that show similar low-frequency variations (Figure 8). The underestimation of the WTC trend by Jason-3 radiometer compared to the CDRs, SARAL/AltiKa and Sentinel-3A suggests that Jason-3 overestimates the GMSL estimates by about  $0.5 \text{ mm}\cdot\text{yr}^{-1}$ . The low-frequency variations of the GMWTC differences show that most of the drift is occurring during the first 2 years of Jason-3's period (Figure 8). The drift of Jason-3's MWR-derived WTC is currently under investigation by the JPL team in charge of the MWR instrumental monitoring and could be related to either a trend or a jump on one or two brightness temperature channels, consistent with the observed trend on the WTC but still to be confirmed (Shannon Brown, January 2023, personal communication). Indeed, on the contrary to Jason-1 and Jason-2, Jason-3's MWR does not benefit yet from the long term comparison to SSMI FCDR that eventually allows for a fine correction of residual trends (see Brown, 2013).

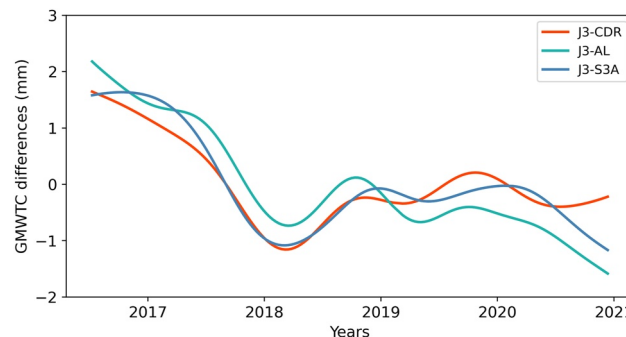


**Figure 8.** Comparison of global mean WTC (GMWTC) differences between Jason-3's MWR, REMSS CDR, SARAL/AltiKa's MWR (AL) and Sentinel-3A's MWR (S3A) over the period from 05 07 2016 to 17 12 2020. For each time series, a 1-year low-pass filter has been applied and the temporal average has been removed. GMWTC differences impact the global mean sea level differences with the opposite sign.

## 6. Conclusion

Analyzing the role of the MWR WTC long-term uncertainty on the GMSL trend uncertainty, we show that the WTC is responsible for about 10% of the uncertainty variance over the full altimetry record and for about 40% over the last 10 years of the record. Using CDR TCWV data and an updated polynomial model with robust coefficient estimates, a new WTC is computed and applied to the altimetric sea level data. Over the full altimetry period, the REMSS CDR-derived GMWTC decreases twice as fast as the altimeters' MWR-based GMWTC. Using an empirical approach, we estimate the CDR-derived GMWTC trend uncertainty to be about  $0.05 \text{ mm.yr}^{-1}$ . This assessment would be strengthened by a more thorough description of the uncertainties of the input water vapor CDRs, via variance-covariance matrices for instance. Indeed, the uncertainty information on the water vapor CDRs is limited to the global mean trend uncertainty based on Schröder et al. (2016) and to an upper-bound estimate of the water vapor data uncertainty from Schröder et al. (2013). Besides, the validity of the trend uncertainty estimated from Schröder et al. (2016) for our study is not straightforward due to different periods of study and different computational methods. Concerning the propagation of the polynomial model uncertainties, our analysis only takes into account the polynomial coefficient uncertainties, without considering the coefficient correlations. Further improvements could also include other sources of uncertainty, such as the polynomial truncation and the neglected effect of the temperature dependency.

Compared to the reference GMSL computed with the altimeters' MWR-based WTC, the GMSL corrected with a CDR-derived WTC exhibits a larger trend, except over the Jason-3 period. The CDR-derived GMWTCs are closer to the Sentinel-3A and SARAL-AltiKa altimeters' MWR-based GMWTC, suggesting a drift of a few tenth of  $\text{mm.yr}^{-1}$  in the Jason-3 MWR measurements that tends to overestimate the GMSL trend over the last few years. This partly explains the non-closure of the GMSL budget observed since 2016 by comparing altimetry with satellite gravimetry and Argo oceanographic data (Barnoud et al., 2021; Chen et al., 2020).

The use of the CDR-derived GMWTC increases the GMSL trend by up to 10% and reduces its uncertainty variance by up to 27% depending on the CDR data set and period of time. As pointed out at the end of Section 5.4, this study allows to exhibit a potential artificial trend of about  $0.5 \text{ mm.yr}^{-1}$  on Jason-3, compliant with the Jason-3 system requirement and at the limit of the current trend detection system based on the monitoring of vicarious calibration targets. However, in order to get closer to the more stringent scientific requirements defined for climate-related studies, we advocate the use of CDR-derived WTC, more stable than the altimeters' MWR-based WTC, even if future improvements on the computation of a CDR-derived WTC are expected (direct use of monthly estimation of the polynomial coefficients, potentially a set of coefficients per zonal latitude bands). Note that the latest generation of MWR for altimetry as the Advanced Microwave Radiometer for Climate on board Jason-6 includes a cold-sky calibration similar to the one used on board SSM/I series and is thus expected to be much more stable. But even in that case, we believe that the CDR-derived WTC could provide a useful comparison and any differences between the operational WTC and the CDR-derived WTC will help to better quantify the uncertainties.

As an example of climate-related application, Hakuba et al. (2021) and Marti et al. (2022) have estimated the Earth's energy imbalance from satellite altimetry and gravimetry data with a level of accuracy of  $0.13\text{--}0.15 \text{ W.m}^{-2}$  on decadal time scales. However, an uncertainty below  $0.1 \text{ W.m}^{-2}$  at decadal time scales would be necessary to monitor the variations due to large volcanic eruptions, variations in natural forcing and internal variability or expected future mitigation of anthropogenic emissions (Meyssignac, Boyer, et al., 2019). Such studies could benefit from the long-term stability of the water vapor CDRs.

The CDR-derived WTC time series computed in this study are available online at <https://doi.org/10.24400/527896/a01-2022.018>.

## Appendix A: TCWV, GMWTC and GMSL Trend Estimates and Uncertainties

Table A1 summarizes the TCWV, GMWTC, and GMSL trends and their standard uncertainties computed over each altimetric mission and over the full altimetric period.

**Table A1**  
*Trends of Total Column Water Vapor ( $\text{kg}\cdot\text{m}^{-2}\cdot\text{yr}^{-1}$ ), Global Mean Wet Troposphere Correction ( $\text{mm}\cdot\text{yr}^{-1}$ ) and Global Mean Sea Level ( $\text{mm}\cdot\text{yr}^{-1}$ ) and Associated Standard Uncertainties, Depending on the Source of Wet Troposphere Correction, Computed for Each Altimetric Mission and Over the Full Altimetric Period*

Mission	TOPEX/Poseidon	Jason-1	Jason-2	Jason-3	All
Period	29 09 1992– 24 04 2002	24 04 2002– 19 10 2008	19 10 2008– 07 11 2014	19 10 2008– 26 05 2016	29 09 1992– 28 06 2021
TCWV <sub>REMISS</sub> (1)	0.074 ± 0.006	-0.053 ± 0.006	0.029 ± 0.006	0.123 ± 0.006	0.049 ± 0.006
TCWV <sub>HOAPS</sub> (1)	0.063 ± 0.007	-0.061 ± 0.007	0.043 ± 0.007	0.036 ± 0.007	0.036 ± 0.007
GMWTC <sub>MWR</sub> (1)	-0.31 ± 0.17	0.38 ± 0.34	0.08 ± 0.36	-0.56 ± 0.29	-0.05 ± 0.10
GMWTC <sub>REMISS_LF+MWR_HF</sub> (1)	-0.45 (+45%) ± 0.05 (-91%)	0.33 (-13%) ± 0.05 (-94%)	-0.19 (-338%) ± 0.05 (-94%)	-0.76 (+36%) ± 0.05 (-93%)	-0.30 (+500%) ± 0.05 (-69%)
GMWTC <sub>HOAPS_LF+MWR_HF</sub> (1)	-0.38 (+23%) ± 0.05 (-91%)	0.38 (0%) ± 0.05 (-94%)	-0.27 (-438%) ± 0.05 (-94%)	-0.22 (+340%) ± 0.05 (-69%)	-0.22 (+340%) ± 0.05 (-69%)
GMWTC <sub>REMISS_LF-GMWTC<sub>MWR_LF</sub></sub>	-0.14 ± 0.18	-0.05 ± 0.20	-0.27 ± 0.20	-0.19 ± 0.19	-0.25 ± 0.10
GMWTC <sub>HOAPS_LF-GMWTC<sub>MWR_LF</sub></sub>	-0.07 ± 0.18	0.00 ± 0.20	-0.35 ± 0.20	-0.17 ± 0.10	-0.17 ± 0.10
GMSL <sub>MWR</sub> with and without WTC <sub>MWR</sub> low-frequency uncertainty (2)	2.77 ± 0.68	2.48 ± 0.44	3.40 ± 0.41	4.17 ± 0.34	2.84 ± 0.27
	± 0.66 (-6%)	± 0.40 (-17%)	± 0.36 (-23%)	± 0.28 (-32%)	± 0.25 (-14%)
GMSL <sub>REMISS_LF+MWR_HF</sub>	2.90 (+5%) ± 0.66 (-6%)	2.53 (+2%) ± 0.40 (-17%)	3.67 (+8%) ± 0.36 (-23%)	4.36 (+5%) ± 0.29 (-27%)	3.10 (+9%) ± 0.26 (-7%)
GMSL <sub>HOAPS_LF+MWR_HF</sub>	2.84 (+3%) ± 0.66 (-6%)	2.48 (0%) ± 0.40 (-17%)	3.76 (+11%) ± 0.36 (-23%)	3.71 (-8%) ± 0.50 (-14%)	3.01 (+6%) ± 0.26 (-7%)

*Note.* The percentages indicate the relative change in trend and in uncertainty variance with respect to the use of the classical WTC based on the altimeters' MWR. Differences between CDR-derived and MWR-based GMWTC are also given, corresponding to the quantities plotted on Figure 6. (1) For TCWV and GMWTC trends, only low-frequency uncertainties are included in the trend uncertainty computation as no estimates are available for high-frequency uncertainties. (2) The MWR-based GMSL uncertainty is computed once using the full uncertainty budget and once setting the WTC<sub>MWR</sub> low-frequency uncertainty to zero. The latter estimate corresponds to the lowest uncertainty that could be reached if the WTC was perfectly stable.

## Data Availability Statement

This study exclusively uses open data sets. The ECMWF ERA5 WTC and TCWV data are distributed by C3S (<https://cds.climate.copernicus.eu/cdsapp/#/dataset/reanalysis-era5-pressure-levels-monthly-means>). The REMSS CDR TCWV data are available at <http://www.remss.com/measurements/atmospheric-water-vapor/tpw-1-deg-product/>. The HOAPS CDR TCWV data are available at <https://wui.cmsaf.eu/safira/action/viewProduktDetails?eid=21864&fid=23>. The altimeter products were produced and distributed by AVISO+ (<https://www.aviso.altimetry.fr/>), as part of the Ssalto ground processing segment.

## Acknowledgments

The authors thank Rémi Jugier and Robin Fraudeau from Magellium for their help in this study. We also thank the reviewers for their careful reading and their comments that helped improve and clarify the manuscript. This work was funded by the French Centre national d'études spatiales (CNES) in the framework of the SALP contract. We particularly thank Thierry Guinle and Gérald Dibarboure from CNES for supporting this study.

## References

- Ablain, M., Meyssignac, B., Zawadzki, L., Jugier, R., Ribes, A., Spada, G., et al. (2019). Uncertainty in satellite estimates of global mean sea-level changes, trend and acceleration. *Earth System Science Data*, 11(3), 1189–1202. <https://doi.org/10.5194/essd-11-1189-2019>
- Andersson, A., Graw, K., Schröder, M., Fennig, K., Liman, J., Bakan, S., et al. (2017). *Hamburg ocean atmosphere parameters and fluxes from satellite data—HOAPS 4.0*. Satellite Application Facility on Climate Monitoring (CM SAF). [https://doi.org/10.5676/EUM\\_SAF\\_CM/HOAPS/V002](https://doi.org/10.5676/EUM_SAF_CM/HOAPS/V002)
- Barnoud, A., Pfeffer, J., Guérou, A., Frery, M.-L., Siméon, M., Cazenave, A., et al. (2021). Contributions of altimetry and Argo to non-closure of the global mean sea level budget since 2016. *Geophysical Research Letters*, 48(14), e2021GL092824. <https://doi.org/10.1029/2021gl092824>
- Bean, B. R., & Dutton, E. J. (1966). *Radio meteorology* (Vol. 92). Superintendent of Documents, US Government Print.
- Bevis, M., Businger, S., Chiswell, S., Herring, T. A., Anthes, R. A., Rocken, C., & Ware, R. H. (1994). GPS meteorology: Mapping zenith wet delays onto precipitable water. *Journal of Applied Meteorology*, 33(3), 379–386. [https://doi.org/10.1175/1520-0450\(1994\)033<0379:gmmzwd>2.0.co;2](https://doi.org/10.1175/1520-0450(1994)033<0379:gmmzwd>2.0.co;2)
- Brown, S. (2013). Maintaining the long-term calibration of the Jason-2/OSTM advanced microwave radiometer through intersatellite calibration. *IEEE Transactions on Geoscience and Remote Sensing*, 51(3), 1531–1543. <https://doi.org/10.1109/tgrs.2012.2213262>
- Brown, S., Desai, S., Keihm, S., & Ruf, C. (2006). JMR noise diode stability and recalibration methodology after three years on-orbit. *2006 IEEE MicroRad*, 7-12. <https://doi.org/10.1109/micrad.2006.1677053>
- Brown, S., Desai, S., Lu, W., & Tanner, A. (2007). On the long-term stability of microwave radiometers using noise diodes for calibration. *IEEE Transactions on Geoscience and Remote Sensing*, 45(7), 1908–1920. <https://doi.org/10.1109/tgrs.2006.888098>
- Chen, J., Tapley, B., Wilson, C., Cazenave, A., Seo, K.-W., & Kim, J.-S. (2020). Global ocean mass change from GRACE and GRACE follow-on and altimeter and Argo measurements. *Geophysical Research Letters*, 47(22), e2020GL090656. <https://doi.org/10.1029/2020GL090656>
- Davis, J. L., Herring, T. A., Shapiro, I. I., Rogers, A. E. E., & Elgered, G. (1985). Geodesy by radio interferometry: Effects of atmospheric modeling errors on estimates of baseline length. *Radio Science*, 20(6), 1593–1607. <https://doi.org/10.1029/rs020i006p01593>
- Fennig, K., Schröder, M., & Hollmann, R. (2017). Fundamental climate data record of microwave imager radiances, edition 3. *Satellite Application Facility on Climate Monitoring (CM SAF)*. [https://doi.org/10.5676/EUM\\_SAF\\_CM/FCDR\\_MWI/V003](https://doi.org/10.5676/EUM_SAF_CM/FCDR_MWI/V003)
- Fennig, K., Schröder, M., Andersson, A., & Hollmann, R. (2020). A fundamental climate data record of SMMR, SSM/I, and SSMIS brightness temperatures. *Earth System Science Data*, 12(1), 647–681. <https://doi.org/10.5194/essd-12-647-2020>
- Fernandes, M. J., Lázaro, C., & Vieira, T. (2021). On the role of the troposphere in satellite altimetry. *Remote Sensing of Environment*, 252, 112149. <https://doi.org/10.1016/j.rse.2020.112149>
- Goldhirsh, J., & Rowland, J. R. (1982). A tutorial assessment of atmospheric height uncertainties for high-precision satellite altimeter missions to monitor ocean currents. *IEEE Transactions on Geoscience and Remote Sensing*, 20(4), 418–434. <https://doi.org/10.1109/tgrs.1982.350408>
- Guérou, A., Meyssignac, B., Prandi, P., Ablain, M., Ribes, A., & Bignalet-Cazalet, F. (2022). Current observed global mean sea level rise and acceleration estimated from satellite altimetry and the associated uncertainty. <https://doi.org/10.5194/egusphere-2022-330>
- Gutenstein, M., Fennig, K., Schröder, M., Trent, T., Bakan, S., Roberts, J. B., & Robertson, F. R. (2021). Intercomparison of freshwater fluxes over ocean and investigations into water budget closure. *Hydrology and Earth System Sciences*, 25(1), 121–146. <https://doi.org/10.5194/hess-25-121-2021>
- Hakuba, M. Z., Frederikse, T., & Landerer, F. W. (2021). Earth's energy imbalance from the ocean perspective (2005–2019). *Geophysical Research Letters*, 48(16), e2021GL093624. <https://doi.org/10.1029/2021gl093624>
- Hersbach, H., Bell, B., Berrisford, P., Biavati, G., Horányi, A., Muñoz Sabater, J., et al. (2019). *Era5 monthly averaged data on pressure levels from 1979 to present*. Copernicus Climate Change Service (C3S) Climate Data Store (CDS). <https://doi.org/10.24381/CDS.6860A573>
- Jugier, R., Ablain, M., Fraudeau, R., Guérou, A., & Féménias, P. (2022). On the uncertainty associated with detecting global and local mean sea level drifts on sentinel-3A and sentinel-3B altimetry missions. *Ocean Science*, 18(5), 1263–1274. <https://doi.org/10.5194/os-18-1263-2022>
- Keihm, S. J., Zlotnicki, V., & Ruf, C. S. (2000). TOPEX microwave radiometer performance evaluation, 1992–1998. *IEEE Transactions on Geoscience and Remote Sensing*, 38(3), 1379–1386. <https://doi.org/10.1109/36.843032>
- Kerr, D. E. (1951). *Propagation of short radio waves*. Institution of Electrical Engineers.
- Legeais, J.-F., Ablain, M., & Thao, S. (2014). Evaluation of wet troposphere path delays from atmospheric reanalyses and radiometers and their impact on the altimeter sea level. *Ocean Science*, 10(6), 893–905. <https://doi.org/10.5194/os-10-893-2014>
- Legeais, J.-F., Meyssignac, B., Faugère, Y., Guérou, A., Ablain, M., Pujol, M.-I., et al. (2021). Copernicus sea level space observations: A basis for assessing mitigation and developing adaptation strategies to sea level rise. *Frontiers in Marine Science*, 8, 704721. <https://doi.org/10.3389/fmars.2021.704721>
- Marti, F., Blazquez, A., Meyssignac, B., Ablain, M., Barnoud, A., Fraudeau, R., et al. (2022). Monitoring the ocean heat content change and the Earth energy imbalance from space altimetry and space gravimetry. *Earth System Science Data*, 14(1), 229–249. <https://doi.org/10.5194/essd-14-229-2022>
- Meyssignac, B., Boyer, T., Zhao, Z., Hakuba, M. Z., Landerer, F. W., Stammer, D., et al. (2019). Measuring global ocean heat content to estimate the Earth energy imbalance. *Frontiers in Marine Science*, 6, 432. <https://doi.org/10.3389/fmars.2019.00432>
- Meyssignac, B., de Conto, R., Ribes, A., Slangen, A., Richter, K., Ablain, M., et al. (2019). How accurate is accurate enough? In *Ocean surface topography science team meeting*. Retrieved from [https://ostst.aviso.altimetry.fr/fileadmin/user\\_upload/OSTST2019/OPEN\\_11\\_2019\\_how\\_accurate.pdf](https://ostst.aviso.altimetry.fr/fileadmin/user_upload/OSTST2019/OPEN_11_2019_how_accurate.pdf)
- Remote Sensing Systems. (2016). Monthly mean total precipitable water data set on a 1 degree grid made from remote sensing systems version-7 microwave radiometer data, V07r01. Retrieved from [www.remss.com](http://www.remss.com)



- Rüeger, J. M. (2002). Refractive index formulae for radio waves. In *Proceedings of the fig XXII international congress* (Vol. 113).
- Schelleng, J. C., Burrows, C. R., & Ferrell, E. B. (1933). Ultra-short-wave propagation. *Proceedings of the Institute of Radio Engineers*, 21(3), 427–463. <https://doi.org/10.1109/jrproc.1933.227639>
- Schröder, M., Jonas, M., Lindau, R., Schulz, J., & Fennig, K. (2013). The CM SAF SSM/I-based total column water vapor climate data record: Methods and evaluation against re-analyses and satellite. *Atmospheric Measurement Techniques*, 6(3), 765–775. <https://doi.org/10.5194/amt-6-765-2013>
- Schröder, M., Lockhoff, M., Forsythe, J. M., Cronk, H. Q., Haar, T. H. V., & Bennartz, R. (2016). The GEWEX water vapor assessment: Results from intercomparison, trend, and homogeneity analysis of total column water vapor. *Journal of Applied Meteorology and Climatology*, 55(7), 1633–1649. <https://doi.org/10.1175/jamc-d-15-0304.1>
- Smith, E., & Weintraub, S. (1953). The constants in the equation for atmospheric refractive index at radio frequencies. *Proceedings of the IRE*, 41(8), 1035–1037. <https://doi.org/10.1109/jrproc.1953.274297>
- Stum, J., Sicard, P., Carrere, L., & Lambin, J. (2011). Using objective analysis of scanning radiometer measurements to compute the water vapor path delay for altimetry. *IEEE Transactions on Geoscience and Remote Sensing*, 49(9), 3211–3224. <https://doi.org/10.1109/tgrs.2011.2104967>
- Thao, S., Eymard, L., Obligis, E., & Picard, B. (2014). Trend and variability of the atmospheric water vapor: A mean sea level issue. *Journal of Atmospheric and Oceanic Technology*, 31(9), 1881–1901. <https://doi.org/10.1175/jtech-d-13-00157.1>
- Weatherhead, E. C., Reinsel, G. C., Tiao, G. C., Meng, X.-L., Choi, D., Cheang, W.-K., et al. (1998). Factors affecting the detection of trends: Statistical considerations and applications to environmental data. *Journal of Geophysical Research*, 103(D14), 17149–17161. <https://doi.org/10.1029/98jd00995>
- Zawadzki, L., & Ablain, M. (2016). Accuracy of the mean sea level continuous record with future altimetric missions: Jason-3 vs. Sentinel-3a. *Ocean Science*, 12(1), 9–18. <https://doi.org/10.5194/os-12-9-2016>